Temporal dependence of the mass-ablation rate in uv-laser-irradiated spherical targets

P. A. Jaanimagi,* J. Delettrez, B. L. Henke,* and M. C. Richardson
Laboratory for Laser Energetics, University of Rochester, 250 East River Road, Rochester, New York 14623-1299
(Received 6 January 1986)

In this paper we present new measurements of thermal transport in spherical geometry using time-resolved x-ray spectroscopy. We determine the time dependence of the mass-ablation rate by following the progress of the ablation surface through thin layers of material embedded at various depths below the surface of the target. These measurements, made with 6 and 12 uv (351 nm) beams from the OMEGA laser system of the Laboratory for Laser Energetics of the University of Rochester, are compared to previous thermal transport data and to detailed hydrodynamic code simulations. We find agreement with code results for the scaling of the mass-ablation rate with absorbed intensity, but measure larger absolute values than predicted. This finding is interpreted as being the result of irradiation nonuniformities on target. The sharp decrease in the mass-ablation rate after the peak of the laser pulse predicted in simulations is consistent with experimental observations.

I. INTRODUCTION

Thermal transport in spherical targets uniformly irradiated with multiple, nanosecond-duration laser beams has been a topic of much theoretical[1] and experimental interest.[2–6] An understanding of thermal transport processes in laser fusion plasmas is important in that they impact directly on laser-induced ablation processes which drive the implosion of direct-drive laser fusion targets. The direct measurement of the transport of thermal energy from the absorption region to the ablation surface is not possible. However, the mass-ablation rate $\dot{m}$ (g/cm^{2}s) which is dependent on the thermal transport can be measured through a variety of diagnostics, such as plasma velocity and x-ray spectroscopic techniques. In effect, $\dot{m}$ is a measure of the depth of material penetrated by the heat front during the laser pulse.

There is a growing body of experimental measurements of $\dot{m}$, some of which appears to suggest that the transport of thermal energy is inhibited. Computer simulations of these experiments place an upper limit on the heat flux q,[7] such that $q=\min(q_{\rm cl}, fq_{\rm fs})$, where $q_{\rm cl}$ is the classical value, $q_{\rm fs}$ is the free-streaming limit and f is referred to as the flux limiter. Experiments in spherical geometry have inferred various levels of flux inhibition. For $\lambda=1.05$ μm laser irradiation[2–5] values range from as low as $f=0.06$ to fluxes in excess of the free-streaming limit. In Ref. 4, a low-temperature foot on the heat front was postulated which cannot be explained with a simple flux-limited inhibition model. At $\lambda=0.53$ μm, a flux limiter of $f>0.1$ has been inferred.[2] In experiments at $\lambda=0.35$ μm, markedly different values of $\dot{m}$ and of its scaling with absorbed intensity I_A were estimated depending on whether they were inferred from charge-collector or time-integrated x-ray spectroscopy measurements.[6]

This broad range of inferred flux limiters from apparently similar experiments is difficult to reconcile. The inconsistency could be due to differences in experimental parameters such as laser pulse shape and irradiation geometry and uniformity. Other factors such as the shorter scale lengths on smaller targets and the onset of resonant absorption at higher intensities will also affect thermal transport. Further, important consideration must be given to the influence of time-dependent effects.

In this paper we discuss the time dependence of the mass-ablation rate and its scaling with absorbed intensity. In Sec. II we present simulations of the mass-ablation rate, emphasizing its time dependence during the laser pulse. This is followed in Sec. III with our experimental results from time-resolved x-ray spectroscopy.

II. COMPUTER SIMULATIONS OF THE MASS-ABLATION RATE

Simulations of the interaction of intense 351-nm laser radiation with spherical targets were made with the one-dimensional Lagrangian code LILAC.[8] In the simulations a 2.5 TW peak power, 600-ps [full width at half maximum (FWHM)] Gaussian laser pulse was tangentially focused on 404-μm-diam targets, producing an average incident intensity of $I_0=5\times10^{14}$ W/cm^2. The hydrocode simulations include ray tracing using the azimuthally averaged laser spatial profile, radiation transport with local thermodynamic equilibrium (LTE) opacities and heat flux as the harmonic mean of $q_{\rm cl}$ and $fq_{\rm fs}$. Simulations were run for a variety of flux limiters ranging from $f=0.02$ to 0.4. From these code calculations we can obtain the instantaneous mass-ablation rate during a single laser pulse as a function of the instantaneous absorbed intensity as referenced to the original target diameter. The case for a flux limiter of $f=0.1$ is illustrated in Fig. 1 for a solid glass sphere and a 6-μm-thick glass shell target. The mass-ablation rate was determined by following the progress of the 500-eV isotherm as referenced to the original Lagrangian frame:

$$\dot{m}=\rho\Delta r/\Delta\tau\ , \tag{1}$$

where ρ is the material density, and Δr is the thickness of material progressively heated to 500 eV in a time $\Delta\tau$. The 500-eV isotherm was chosen as a characteristic tempera-

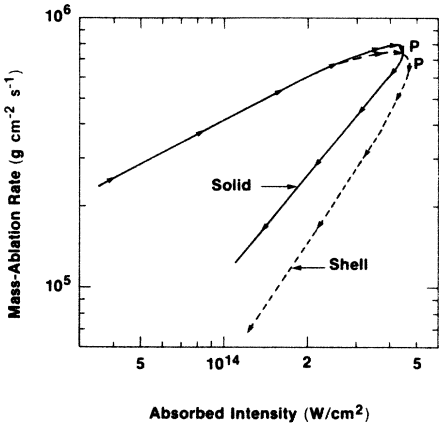

FIG. 1. LILAC simulation for the instantaneous mass-ablation rate [from Eq. (1)] vs the instantaneous absorbed intensity during a single laser pulse, $I_0=5\times10^{14}$ W/cm^2, $f=0.1$ on 404-μm-diam glass targets; solid target (——), 6-μm wall shell target (— — —). Arrows mark 100-ps time intervals starting at 200 ps code time and P denotes the peak of the laser pulse at 773 ps.

ture for Si line emission in the 2.0—2.5 keV range which was used as a diagnostic in the experiments described later. $\dot{m}(t)$ derived from the 300-eV or 1-keV isotherms is essentially the same as for the 500-eV isotherm, with peak values occurring marginally earlier and later in time, respectively. This is characteristic of the steep classical heat front in the overdense material.

The noteworthy features of the curves in Fig. 1 are (i) that $\dot{m}$ does not have the same scaling with absorbed intensity (I_A) on the rising and falling edges of the laser pulse and (ii) that the peak value of $\dot{m}$ is achieved prior to the peak values of both the incident and absorbed intensities. These features are even more pronounced for the case of an imploding glass shell target as compared to the solid target. A similar dependence of $\dot{m}$ on I_A was observed in simulations with other flux limiters as well as for targets of different diameters and different Z.

In a general sense, an empirical mathematical relationship between $\dot{m}$ and I_0 is valuable for understanding thermal transport, and would aid laser fusion target design. However, our efforts to use the simulations to generate scaling laws of the form $\dot{m}\propto I_A^x R_A^y$ (as in Ref. 1), where R_A is the radius of the 500-eV isotherm, have been successful only for individual cases and then only for imploding-shell targets. On solid glass spheres the excursion of R_A during the laser pulse may range up to 30% of the initial target radius, but it cannot account for the observed decrease in $\dot{m}$. Larger excursions are observed for higher intensity laser pulses (5×10^{15} W/cm^2) and for smaller (200 μm) diameter targets.

At $\lambda=351$ mn the predominant absorption mechanism is inverse bremsstrahlung in the subcritical region, and we can define an energy deposition radius R_D as the weighted average absorption radius. Typically R_D lies between the critical and quarter-critical density radii, but inside the peak temperature ($\nabla T=0$) surface. Defining $\Delta R=R_D-R_A$ as the separation between the energy deposition and ablation surfaces, we find the scaling laws for glass targets:

$$\dot{m}\propto I_A^{0.5}R_A^{1.4}\Delta R^{-0.06} \quad \text{for } f=0.02\ ,$$

$$\dot{m}\propto I_A^{0.65}R_A^{1.3}\Delta R^{-0.3} \quad \text{for } f=0.04\ ,$$

and

$$\dot{m}\propto I_A^{1.0}R_A^{1.0}\Delta R^{-0.73} \quad \text{for } f=0.4\ .$$

The scaling at $f=0.1$ is similar to that at $f=0.4$. The magnitude of ΔR is partially dependent on the size and constituents of the target. For moving-shell targets ΔR increases monotonically throughout the laser pulse, but for solid spheres ΔR is approximately constant after the peak of the laser pulse. We also note that ΔR is proportional to the density scale length L_D at R_D, and perhaps L_D is a more meaningful parameter for the scaling laws, as it affects energy deposition in the corona directly. Another factor which contributes to decreasing $\dot{m}$ is the fact that the fraction of the absorbed energy deposited outside the $\nabla T=0$ surface increases during the laser pulse.

As suggested in Ref. 1, laser energy absorption by inverse bremsstrahlung leads to reduced $\dot{m}$ and reduced ablation pressure compared to an energy dump at critical density. More of the laser energy is dissipated at subcritical densities, flowing more directly into blow-off kinetic energy. With respect to the above scaling laws, inverse bremsstrahlung implies a larger ΔR since R_D is greater than the critical-density radius. From Ref. 1 we note that the ablation pressure has a much weaker scaling with radius than $\dot{m}$ does, and our simulations do show that the pressure at the 500-eV isotherm scales with I_A on both the leading and trailing edges of the pulse for the solid targets.

In light of the above simulations, care must be taken when plotting $\dot{m}$ obtained from time-resolved x-ray spectroscopy versus absorbed intensity. Using a pulse-averaged I_A will result in an underestimate in the value of $\dot{m}(I_A)$. To avoid such problems the time-varying values of $\dot{m}$ should be plotted versus the instantaneous value of I_A.

III. EXPERIMENTS

The primary diagnostic for our mass-ablation rate measurements was time-resolved x-ray spectroscopy.[9,10] The experiments were carried out using 6 and 12 uv ($\lambda=351$ nm) beams of the OMEGA laser system of the Laboratory for Laser Energetics at the University of Rochester at incident irradiances of $I_0=(1-4)\times10^{14}$ W/cm^2. The laser pulse had a Gaussian temporal profile with a pulsewidth of 600—750 ps FWHM. Two types of targets were used in these studies. One set consisted of empty glass microballoons ($\sim$230 μm diameter) with a 1.0-μm-thick wall. These shells were coated with parylene (CH) (1.0—8.0 μm thick) and then overcoated with a 150-Å layer of Au to provide an initial x-ray time marker. The Au layer thickness was increased to 300 Å for the 12-beam target shots. The second set of targets

were solid glass spheres (~ 200 μm diameter) coated with three layers: 1.5 μm CH, 0.05 μm Al, and 1.5 μm CH.[11]

An elliptically curved pentaerythritol (PET) crystal analyzer was used to disperse the x-ray spectrum (1.7—2.7 keV range) onto the slit of the x-ray streak camera. Spectral and temporal resolutions were $E/\Delta E \sim 600$ and 15 ps, respectively. Representative perspective plots of the x-ray intensity from streak records for 6- and 12-beam shots on the imploding targets are presented in Fig. 2 showing the Au M-band emission and the Si line emission. The time of occurrence of the implosion can be deduced from the peak in the x-ray continuum emission. This x-ray burst is characteristic of the higher temperatures and densities achieved during the stagnation of the glass shell and lasts ~ 150 ps. The mass-ablation rate through the CH layers of known thickness was measured from the time delay between the start of the Au or Al line emission to the onset of the Si emission from the glass substrate. In all of the target shots where $\dot{m}$ could be measured, the CH layer ablated during the rising edge of laser pulse. Thicker CH layers (6—8 μm) did not appear to burn through for intensities $<3\times 10^{14}$ W/cm^2.

In order to construct a meaningful plot of $\dot{m}$ versus I_A, we require knowledge of the absorbed laser intensity during the CH burnthrough time of interest. Since we could not measure directly the absorption fraction as a function of time nor relate the x-ray emission to the incident laser pulse, $I_A(t)$ was inferred from careful comparisons of the streak data with the LILAC code simulations. We assumed that, if the overall predicted absorption of the laser energy agreed with the experimental measurement, then the code could be relied upon to predict the instantaneous absorbed laser intensity during the pulse. A flux limiter of $f=0.04$ was required to match the absorbed fractions. We also assumed that the hydrodynamic implosion time predicted by the code for the shell targets was correct. Then, by matching the predicted and experimental implosion times we are able to relate the x-ray emission on the streak record to the incident laser pulse. The accuracy of equating the implosion times was checked by calculating the predicted absorbed laser energy up to a time corresponding to the onset of the Au emission as measured on the streak record. The calculated absorbed laser energy was in the range 3.0 to 5.5 J, Fig. 3, and corresponds to a time window of ~ 80 ps. Conservatively, this implies a 100-ps accuracy in our timing fiducial technique. By including a ± 50-ps jitter in the streak record timing we obtain a timing fiducial with 150-ps accuracy for the solid sphere targets.

In Fig. 4 we present the scaling of the measured mass-

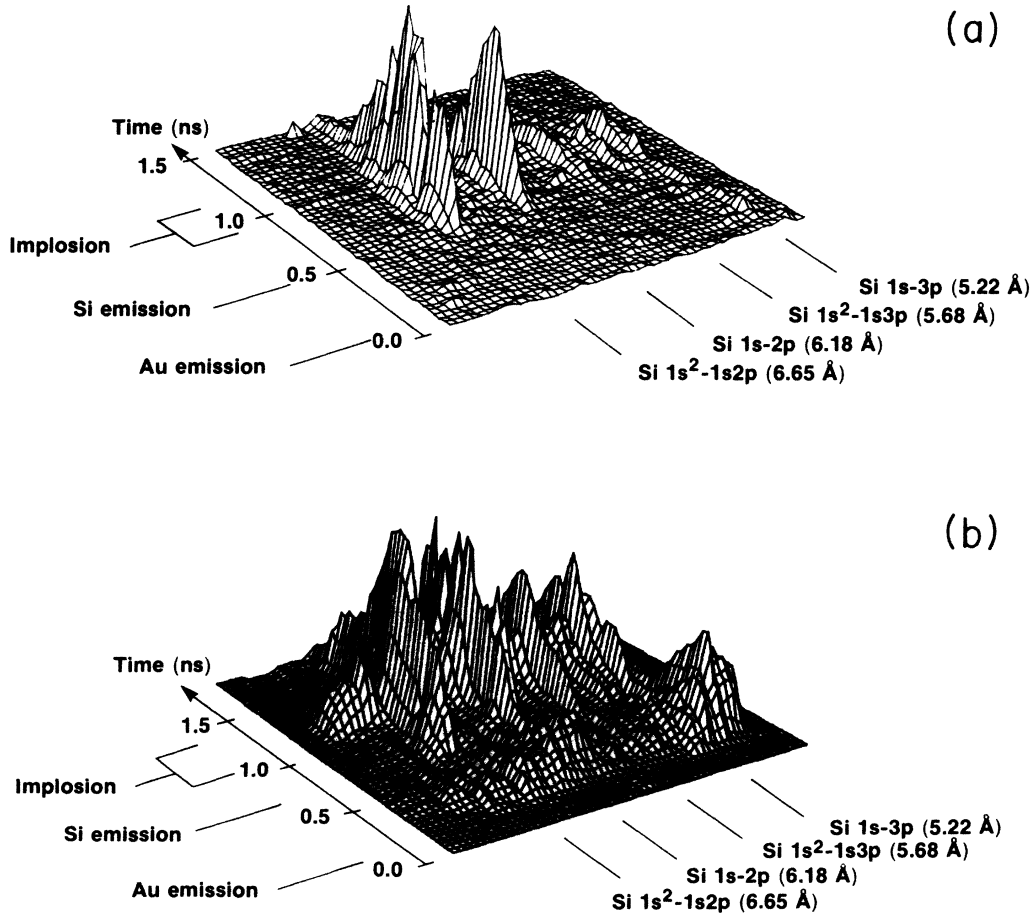

FIG. 2. Perspective plots of the x-ray intensity as recorded by the streak camera. Correction for the spectrometer response function would increase the intensity on the long-wavelength side by 40%. (a) 150 Å Au on 4 μm CH on 1.0-μm glass shell target. Diameter is 229 μm at $I_0=2.8\times 10^{14}$ W/cm^2 with six-beam irradiation. (b) 300 Å Au on 3 μm CH on 1.0-μm glass shell target. Diameter is 289 μm at $I_0=4.2\times 10^{14}$ W/cm^2 with 12-beam irradiation.

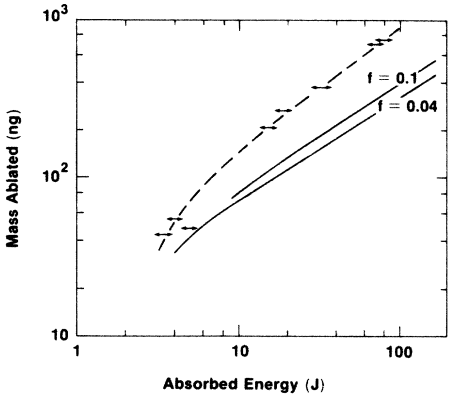

FIG. 3. Ablated mass vs absorbed energy during a single laser pulse for six-beam irradiation of multilayer targets. Solid lines are LILAC simulations for the mass outside the 500-eV isotherm. For the experimental data the total mass outside the glass substrate is assumed to have been ablated. Data points at ~4 J absorbed energy are for the ablation of the outer Au layer only.

ablation rate as a function of the average absorbed laser intensity during the CH burnthrough interval; I_A is derived from the simulations as outlined above. We also include data for $\dot{m}$ for the outer CH layer on the solid targets where I_A is derived using 3 J of absorbed energy for time zero. The time-resolved six-beam data is in excellent agreement with the time-integrated measurements at $I_A = 7.5 \times 10^{13}$ W/cm^2, which was measured for a similar target diameter (Ref. 6). The scaling of $\dot{m}$ with I_A for six-beam irradiation and $I_A \lesssim 10^{14}$ W/cm^2 is in reasonable agreement with code predictions although the magnitude of $\dot{m}$ is ~2 times higher than that predicted for uninhibited transport ($f = 0.4$). The scaling of $\dot{m}$ with I_A derived from the time-integrated x-ray spectroscopy of Ref. 6 is much weaker than that reported here.

A possible cause for the discrepancy between the measured and calculated values of $\dot{m}$ could be the known variances in the intensity distribution across the surface of the target.[12,13] These have been estimated using a three-dimensional superposition code which combines the equivalent target plane intensity distribution of each beam and computes a spherical-harmonic mode decomposition of the intensity distribution on the target surface.[14] An initial assessment of the irradiation uniformity with six uv (351-nm) beams of OMEGA indicates an overall rms nonuniformity of ~50% in the lowest 30 l modes.[12] Alternatively this can be stated as a few percent of the laser energy is absorbed at an intensity greater than three times the average intensity.[15] Further characterization of the irradiation nonuniformities is obtained from x-ray pinhole pictures of solid high-Z (Au) targets irradiated with six beams, which show large-scale intensity variations across the target surface.[16] Time-resolved imaging of the x-ray emission from these targets has also confirmed the existence of discrete hot spots.[16] Given the amount of energy in the hot spots and the sensitivity of our diagnostic (Au emission is detected at the 2% of the total absorbed energy level from Fig. 3), the value of $\dot{m}$ obtained using time-resolved spectroscopy should be characteristic of the absorbed intensity in the hot spots. A shift of our experimental points in Fig. 4 by a factor of 3 in I_A results in reasonable agreement with code predictions for $f = 0.1$. Under the assumption that the laser energy distribution on target is the same for the approximately constant diameter targets used in these studies, the measured scaling of $\dot{m}$ with I_A should be valid. Similarly the discrepancy between the measured and calculated values of the amount of mass ablated during the laser pulse in Fig. 3 can be attributed to the burnthrough of only small areas of the CH coating corresponding to the hot spots in the irradiation pattern.

With 12-beam irradiation the illumination uniformity should be improved and the effects of hot spots on the burnthrough should be commensurately less. Experimentally we do observe a significant decrease in the magnitude of $\dot{m}(I_A)$ (see Fig. 4). Further evidence for the decrease in $\dot{m}$ with the more uniform 12-beam irradiation are the "burnthrough" curves presented in Fig. 5, as measured by the time-integrating channel of the x-ray spec-

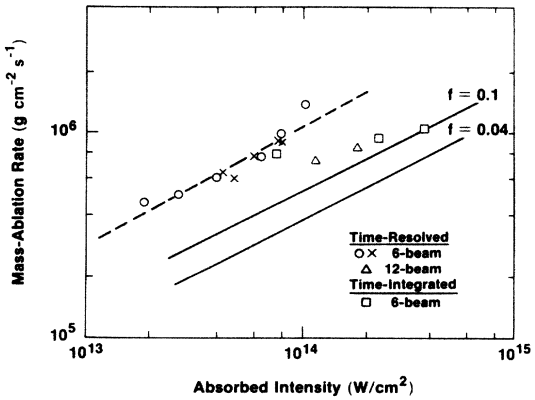

FIG. 4. Mass-ablation rate versus absorbed intensity at $\lambda = 0.351$ μm. Compilation from this study (— — —), time-integrated measurements from Ref. 6, and LILAC simulations at $f = 0.1$ and 0.04 for the rising edge of the pulse.

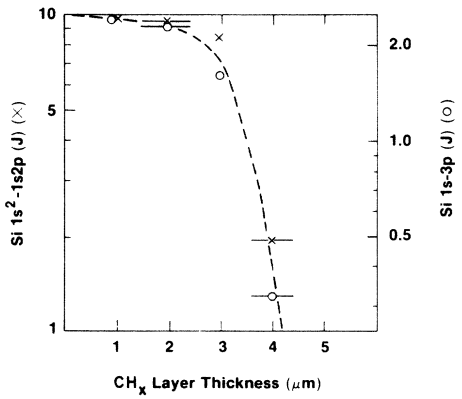

FIG. 5. "Burnthrough" curves for CH and Au/CH on glass targets with 12-beam irradiation at $I_0 = 4.0 \times 10^{14}$ W/cm^2 for the Si He$_\alpha$ (x) and Si H$_\beta$ (0) x-ray resonance lines.

trometer.[10] Here we plot the absolute energy in the Si^{+12} $1s^2$-$1s2p$ and Si^{+13} $1s$-$3p$ lines as a function of CH overcoat thickness. The 300-Å Au layer on two of the targets was assumed to have an areal mass density equivalent to 0.5 μm of CH, although the effective thickness of the Au layer is greater than this due to radiation cooling in the higher-Z material. The projected burnthrough thickness of ≤ 5 μm of CH is much less than the 9 μm of CH interpolated at $I_0 = 3 \times 10^{14}$ W/cm^2 from the six-beam data (Ref. 6). This difference cannot be accounted for strictly by the difference in burnthrough depth between shells and solids, nor by the presence of the thin Au layer on the outside of the targets used in these experiments. Although we have not investigated a very large range of absorbed intensities with 12-beam irradiation, it is our contention that the scaling of $\dot{m}$ with I_A would be the same as for the time-resolved six-beam data.

Although we do not have any direct measurements of the mass-ablation rate on the trailing edge of the laser pulse, we do not observe any Si line emission on the streak records for the six-beam shots on targets with 6- and 8-μm-thick overcoats of CH. This is consistent with the predicted decrease in $\dot{m}$ starting before the peak of the laser pulse as illustrated in Fig. 1. Using the timing fiducial method outlined above we estimate that the onset of the Si line emission for a target with a 4-μm CH overcoat occurs ~ 50 ps before the peak of the laser pulse. If there had been a symmetric scaling of m with I_A on the leading and trailing edges of the pulse, surely we would have observed the Si line emission from the targets with the thicker CH coatings. In addition, if we extrapolate the experimental data in Fig. 3 to the mass of these CH layers, the absorbed laser energy on these target shots was sufficient to produce some Si line emission.

Consideration must also be given to the probability of lateral thermal smoothing of the hot spots in the intensity distribution on the target which appear to dominate the burnthrough and $\dot{m}$ measurements with six-beam irradiation. The amount of smoothing depends on the fractional separation distance $\Delta R/R_0$, where R_0 is the target radius.[17,18] For the imploding targets used in this study, the value of $\Delta R/R_0$ is ~ 0.2 at the peak of the laser pulse. A value of ~ 0.3 is predicted at the peak of the laser pulse for the 90-μm-diam targets irradiated at 10^{15} W/cm^2 in Ref. 6. It is suggested that the lower scaling of $\dot{m}$ with I_A in Ref. 6 is the result of thermal smoothing. This smoothing decreases the magnitude of $\dot{m}$ to a level more characteristic of the average intensity on target.

IV. CONCLUSION

The measurement of the mass-ablation rate in spherical geometry with short-wavelength lasers in influenced significantly by time-dependent effects during the laser pulse.[19] The transport of thermal energy and therefore $\dot{m}$ is affected by the increasing separation between the energy deposition and ablation surfaces. Irradiation nonuniformities also have a significant effect on x-ray spectroscopic measurements of the mass-ablation rate since the burnthrough seems to be dominated by hot spots. Our experimental measurements of m are in agreement with code predictions for the scaling of $\dot{m}$ with I_A on the rising edge of the laser pulse as shown in Fig. 4; only indirect evidence is presented for lower values of $\dot{m}$ on the trailing edge of the laser pulse.

ACKNOWLEDGMENTS

We acknowledge useful discussions with Dr. R. Epstein, Dr. L. Goldman, Dr. A. Hauer, Dr. R. L. McCrory, Dr. J. M. Soures, Dr. S. Skupsky, and Dr. B. Yaakobi and the technical support of Dr. S. A. Letzring, G. Gregory, and the OMEGA operations group. This work was supported by the U. S. Department of Energy Office of Inertial Fusion under Agreements No. DE-A508-82DP40175 and No. DE-FC08-85DP40200 and by the Laser Fusion Feasibility Project at the Laboratory for Laser Energetics which has the following sponsors: Empire State Electric Energy Research Corporation, General Electric Company, New York State Energy Research and Development Authority, Northeast Utilities Service Company, Ontario Hydro, Southern California Edison Company, The Standard Oil Company, and the University of Rochester.

*Permanent address: Lawrence Berkeley Laboratory, University of California, 1 Cyclotron Road, Berkeley, CA 94720.

[1]C. E. Max, C. F. McKee, and W. C. Mead, Phys. Fluids **23**, 1620 (1980).

[2]T. J. Goldsack, J. D. Kilkenny, B. J. MacGowan, P. F. Cunningham, C. L. S. Lewis, M. H. Key, and P. T. Rumsby, Phys. Fluids **25**, 1634 (1982).

[3]J. A. Tarvin, W. B. Fechner, J. T. Larsen, P. D. Rockett, and D. C. Slater, Phys. Rev. Lett. **51**, 1355 (1983).

[4]B. Yaakobi, J. Delettrez, L. M. Goldman, R. L. McCrory, R. Marjoribanks, M. C. Richardson, D. Shvarts, S. Skupsky, J. M. Soures, C. Verdon, D. M. Villeneuve, T. Boehly, R. Hutchinson, and S. Letzring, Phys. Fluids **27**, 516 (1984).

[5]A. Hauer, W. C. Mead, O. Willi, J. D. Kilkenny, D. K. Bradley, S. D. Tabatabaei, and C. Hooker, Phys. Rev. Lett. **53**, 2563 (1984).

[6]B. Yaakobi, O. Barnouin, J. Delettrez, L. M. Goldman, R. Marjoribanks, R. L. McCrory, M. C. Richardson, and J. M. Soures, J. Appl. Phys. **57**, 4354 (1985).

[7]R. C. Malone, R. L. McCrory, and R. L. Morse, Phys. Rev. Lett. **34**, 721 (1975).

[8]For descriptions of earlier versions of LILAC, see E. B. Goldman, Laboratory for Laser Energetics Report No. 16 (unpublished); J. Delettrez and E. B. Goldman, Laboratory for Laser Energetics Report No. 36 (unpublished).

[9]B. L. Henke, H. T. Yamada, and T. J. Tanaka, Rev. Sci. Instrum. **54**, 1311 (1983).

[10]B. L. Henke and P. A. Jaanimagi, Rev. Sci. Instrum **56**, 1537 (1985).

[11]The CH/Al/CH solid-sphere targets were supplied as part of a collaborative effort on thermal transport with Los Alamos National Laboratory (LANL).

[12]M. C. Richardson, S. Skupsky, J. M. Soures, W. Lampeter, S. Tomer, R. Hutchison, M. Dunn, and W. Beich, Conference on Lasers and Electro-optics, 1984, Technical Digest (unpublished).

[13]Laboratory for Laser Energetics, Quarterly Report No. 23, 1985 (unpublished).

[14]M. C. Richardson, S. Skupsky, J. Kelly, L. Iwan, R. Hutchison, R. Peck, R. L. McCrory, and J. M. Soures, Proc. SPIE **380**, 473 (1983).

[15]S. Skupsky (private communication).

[16]S. A. Letzring, M. C. Richardson, P. D. Goldstone, G. Gregory, and G. Eden, Bull. Am. Phys. Soc. **29**, 1318 (1984).

[17]S. E. Bodner, J. Fusion Energy 1, 221 (1981).

[18]S. Skupsky, R. L. McCrory, R. S. Craxton, J. Delettrez, R. Epstein, K. Lee, and C. Verdon, in *Laser Interaction and Related Plasma Phenomena,* edited by H. Hora and G. H. Miley (Plenum, New York, 1984), Vol. 6, p. 751.

[19]The authors thank W. C. Mead of LANL for bringing to our attention a figure which he presented at the 1984 Annual Meeting of the Division of Plasma Physics, Bull. Am. Phys. Soc. **29**, 1380 (1984), which indicated a rollover in $\dot{m}$ in simulations of experiments with Gaussian-shaped pulses at $\lambda = 1\ \mu$m.